Electronic Supplementary Material (ESI) for Journal of Materials Chemistry A.

Self-supported Ni-Co Perselenide Nanorod Array as High-activity Bifunctional Electrodes for Hydrogen Production Hydrazine Fuel Cell

Genxiang Wang[a,b], Junxiang Chen[a], Pingwei Cai[a,b], Jingchun Jia[a], and Zhenhai Wen *[a]

[a]*CAS Key Laboratory of Design and Assembly of Functional Nanostructures, and Fujian Provincial Key Laboratory of Nanomaterials, Fujian Institute of Research on the Structure of Matter, Chinese Academy of Sciences, Fuzhou, Fujian 350002, China*

[b]*University of Chinese Academy of Sciences, Beijing 100049, P. R. China*

*E-mail:wen@fjirsm.ac.cn

Contents

1. Electrochemical neutralization energy

As the pourbaix diagram of water (Figure S15) displayed, the hydrogen evolution reaction (HER) and oxygen evolution reaction (OER) are sensitive to the pH of electrolytes. When the electrolyzer operates in a symmetrical electrolyte, the theoretical applied voltage for water splitting (HER&OER) is always 1.23 V. However, when the HER was performed in acid electrolyte while OER performed in alkaline electrolyte forming a asymmetric-electrolyte electrolyzer, the applied voltage required for water splitting can be calculated based on the corresponding Nernst equations:

For water electrolysis in the alkaline-acid electrolyzer:

HER at the cathode (pH = 0):

$$2H^+ + 2e^- \rightarrow H_2 \qquad \textbf{(R1)}$$

$$E_{HER} = E^{\theta}_{H^+/H_2} - 2.303\frac{RT}{2F}\log\left[\frac{\alpha_{H_2}}{(\alpha_{H^+})^2}\right] = 0\ V - 0.0591 * pH_{cathode} = 0$$

$$(E^{\theta}_{H^+/H_2} = 0\ V\ vs.RHE) \qquad \textbf{(Eq.1)}$$

OER at the anode (pH = 14):

$$4OH^- - 4e^- \rightarrow 2H_2O + O_2 \qquad \textbf{(R2)}$$

$$E_{OER} = E^{\theta}_{O_2/OH^-} - 2.303\frac{RT}{4F}\log\left[\frac{(\alpha_{OH^-})^4}{(\alpha_{H_2O})^2(\alpha_{O_2})}\right] = 1.23\ V - 0.0591 * pH_{anode} = 0.402$$

$$(E^{\theta}_{O_2/OH^-} = 1.23\ V\ vs.RHE) \qquad \textbf{(Eq.2)}$$

The overall reaction for water splitting:

$$4H^+ + 4OH^- \rightarrow 2H_2O + O_2 + 2H_2 \qquad \textbf{(R3)}$$

$$\boldsymbol{V_{theoretical\ required}} = E^{\theta}_{O_2/OH^-} - E^{\theta}_{H^+/H_2} - 2.303\frac{RT}{4F}\log\left[\frac{(\alpha_{H_2O})^2(\alpha_{O_2})(\alpha_{H_2})^2}{(\alpha_{H^+})^4(\alpha_{OH^-})^4}\right]$$

$$= 1.23 - 0.0591 * (pH_{anode} - pH_{cathode}) = \textbf{0.402} \qquad \textbf{(Eq.3)}$$

In these Equations, F is the Faraday constant, 96 485 C mol^{-1}, T is the room temperature (commonly 298.15 K), R is the gas constant (8.314 J mol^{-1} K^{-1}), $pH_{anode} - pH_{cathode}$ is the pH difference (ΔpH) of the anolyte and catholyte, and the $2.303\frac{RT}{F} * \Delta pH$ is equal to the electrochemical neutralization energy deriving from the reaction of hydroxide ion and proton combining to water, which provides an additional energy or voltage for water splitting as presented in **R4**:

$H_3O^+ + OH^- \rightarrow H_2O$ (ΔG = -79 kJ/mol, $\Delta E = \frac{-\Delta G}{nF} = 0.\ 828$ V) (**R4**)

Such asymmetric-electrolyte electrolyte with HER in 0.5 M H_2SO_4 (pH = 0) at cathode and OER in 1.0 M KOH (pH = 14) at anode can be also regarded to form a pH-gradient concentration cell, and a cell voltage of 0.828 V will be produced

For water electrolysis in the alkaline-acid electrolyzer with HzOR replacing OER:

HER at the cathode (pH = 0):

The same as R1

HzOR at the anode (pH = 14):

$N_2H_4 + 4OH^- - 4e^- \rightarrow N_2 + 4H_2O$ **(R5)**

$$E_{HzOR} = E^{\theta}_{HzOR} - 2.303\frac{RT}{4F}\log\left[\frac{(\alpha_{N_2H_4})(\alpha_{OH^-})^4}{(\alpha_{N_2})(\alpha_{H_2O})^4}\right] = -0.33\ V - 0.0591 * pH = -1.158$$

($E^{\theta}_{UOR} = -0.33\ V\ vs.\ RHE$) **(Eq.4)**

The overall reaction:

$N_2H_4 + 4OH^- + 4H^+ \rightarrow N_2 + 4H_2O + 2H_2$ **(R6)**

$$\boldsymbol{V}_{Theory\ required\ or\ open\ circuit}$$

$$= E^{\theta}_{HzOR} - E^{\theta}_{H^+/H_2} - 2.303\frac{RT}{4F}\log\left[\frac{(\alpha_{H_2O})^4(\alpha_{N_2})(\alpha_{H_2})^2}{(\alpha_{N_2H_4})(\alpha_{H^+})^4(\alpha_{OH^-})^4}\right]$$

$$= -0.33 - 0.059 * (pH_{anode} - pH_{cathode}) = \mathbf{-1.158} \quad \textbf{(Eq.5)}$$

Therefore, combined the electrochemical neutralization energy and HzOR, spontaneous H_2 production and power supply can be achieved simultaneously in the electrochemical system, forming an alkaline-acidic hydrazine fuel cell with theoretical overall cell voltage of 1.158 V (0.828 V + (0-(-0.33)) V = 1.158 V).

In such asymmetric-electrolyte device, a bipolar membrane should be employed to prevent the mixture of acid in cathode and alkaline in anode that leads to chemical neutralization. The bipolar membrane is a double-layer membrane that consists of an anion exchanger layer on the cathode side blocking transport of cation and a cation exchanger layer on the anode side of the cell blocking transport of anion, and the K^+ cations are transported to cation exchange layer while SO_4^{2-} anions are transported to anion exchange layer.

2. Production quantification analysis

The produced H_2 in the cathode and N_2 in the anode were collected by drainage method, and the produced H_2 was analyzed by the gas chromatograph equipped with a thermal conductivity detector (TCD). The Faradaic Efficiency calculation formula is expressed as in **Eq.6**,

$$\mathrm{EF} = \frac{\alpha \mathrm{nF}}{Q} \quad \textbf{(Eq.6)}$$

in which α denotes the numbers of transferred electrons (*e.g.* α = 2 for H_2), n denotes the number of moles of the obtained products, F is the faradaic constant, 96 485 C mol^{-1}, and Q denotes the whole passed charge. H_2 and N_2 was collected during the chronopotentiometry experiment conducted at 10 mA cm^{-2} in the homemade cell with

gas collection setup (Figure S13) separated by a bipolar membrane with $Ni_{0.5}Co_{0.5}Se_2$/CC as the bifunctional electrodes in 1 M KOH and 0.5 M H_2SO_4, respectively. Before testing, Ar was introduced in the two chambers for 30 min and then the cell was sealed. The time were recorded every produced 0.5 mL H_2 in the cathode at room temperature (25 °C) and the specific data was presented in Table S5. The total charge Q could be obtained from the applied current and the operating time, namely, Q = I* t, while n could be obtained by the volum of obtained H_2 (V), *i.e.*, n = V/24.5, (24.5 L mol^{-1} is the gas constant at 25 °C), and the volume can be qualitatively determined by the GC analysis. The actual equation can be expressed as following:

$$EF = \frac{\alpha VF}{It*24.5} \quad \textbf{(Eq. 7)}$$

Besides, the H_2 evolution rate ($r(H_2)$, Table S5) was also evaluated based on the equation 8:

$$r(H_2) = \frac{V}{24.5t} \quad \textbf{(Eq. 8)}$$

3. Theoretical Calculation Details

(1) DFT details

Spin-polarized DFT calculations were performed with periodic super-cells under the generalized gradient approximation (GGA) using the Perdew-Burke-Ernzerhof (PBE) functional for exchange-correlation and the ultrasoft pseudopotentials for nuclei and core electrons. The Kohn-Sham orbitals were expanded in a plane-wave basis set with a kinetic energy cutoff of 30 Ry and the charge-density cutoff of 300 Ry. The Fermi-surface effects has been treated by the smearing technique of Methfessel and Paxton, using a smearing parameter of 0.02 Ry. 210 surfaces are cleaved in modeling $NiSe_2$, $CoSe_2$ and $Co_{0.5}Ni_{0.5}Se_2$. The Periodically repeated three layer slab models with 1 x 1 supercell are introduced, while the topmost layer is allowed to relax during the structure optimization until the Cartesian force components acting on each atom were below 10^{-3} Ry/Bohr and the total energy converged to within 10^{-5} Ry. The Brillouin-zones were sampled with a 3×2×1 k-point mesh. The PWSCF codes contained in the Quantum ESPRESSO distribution[1] were used to implement the calculations.

(2) Reaction model.

The total reaction function of basic UzOR is

N_2H_4 (aq) + $4OH^-$(aq) → N_2(g) + $4H_2O$(l) + 4e (**RS1**)

which contains a 4 electrons transfer. The equilibrium potential of RS1 is -0.33 V. Here, for the difficulties in directly modelling N_2H_4 (aq), its Gibbs free energy is deduced by the DFT based free energy of N_2(g), H_2O(l) and OH^-(aq) in utilizing the

condition that RS1 is in equilibrium on -0.33 V. The free energies of $H_2O(l)$ and $OH^-(aq)$ are calculated through the equilibrium of $OH^- + 1/2H_2(g) \rightarrow H_2O(l) + e$ (basic hydrogen oxidation reaction) under U_{RHE}=0 V, where we have:

$G^0[H_2O(l)] - G^0[OH^-(aq)] = G^0[H_2(g)]$ (**S1**)

$G^0[H_2O(l)]$, $G^0[OH^-(aq)]$ and $G^0[H_2(g)]$ are the standard formation Gibbs free energies of $H_2O(l)$, $OH^-(aq)$ and $H_2(g)$. Eq.S1 tells that we can calculate $G^0[H_2(g)]$ in avoid of calculating the $G^0[H_2O(l)]$ and $G^0[OH^-(aq)]$.

Afterwards, on references of the calculations done by Zhou *et al*[2], HzOR follows a consequent deprotonation pathway:

$N_2H_4(aq) + * \rightarrow N_2H_4*$ (**RS2**)

$N_2H_4* + OH^-(aq) \rightarrow N_2H_3* + H_2O(l) + e$ (**RS3**)

$N_2H_3* + OH^-(aq) \rightarrow N_2H_2* + H_2O(l) + e$ (**RS4**)

$N_2H_2* + OH^-(aq) \rightarrow N_2H* + H_2O(l) + e$ (**RS5**)

$N_2H* + OH^-(aq) \rightarrow N_2* + H_2O(l) + e$ (**RS6**)

$N_2* \rightarrow N_2(g)$ (**RS7**)

For each reaction, where the Gibbs free energy of adsorbates are calculated by the $G_{A*} = G_{A*+slab} - G_{slab} + ZPE_{A*}$. ZPE_{A*} stands for the zero point energy (ZPE) of adsorbate A*. The entropy terms are ignored for entropies are usually considered to be zero during the adsorption.

(3) Entropy and zero point energies

(4) Chosen of the active site

As indicated on Figure S16a,c,e, the $Ni_xCo_{1-x}Se_2$ surfaces contain several possible

sites for adsorption. In order to choose the most active sites, the PDOS of all the possible active sites are calculated and depicted on Figure S16b,d,f. Figure S16b,d,f all indicate the sites with highest d states are site 3 and 4. Actually, site 3 and 4 are equivalent sites among the three surfaces. So site 3 are chosen as the active sites when calculating the reaction FEDs.

5. Figures

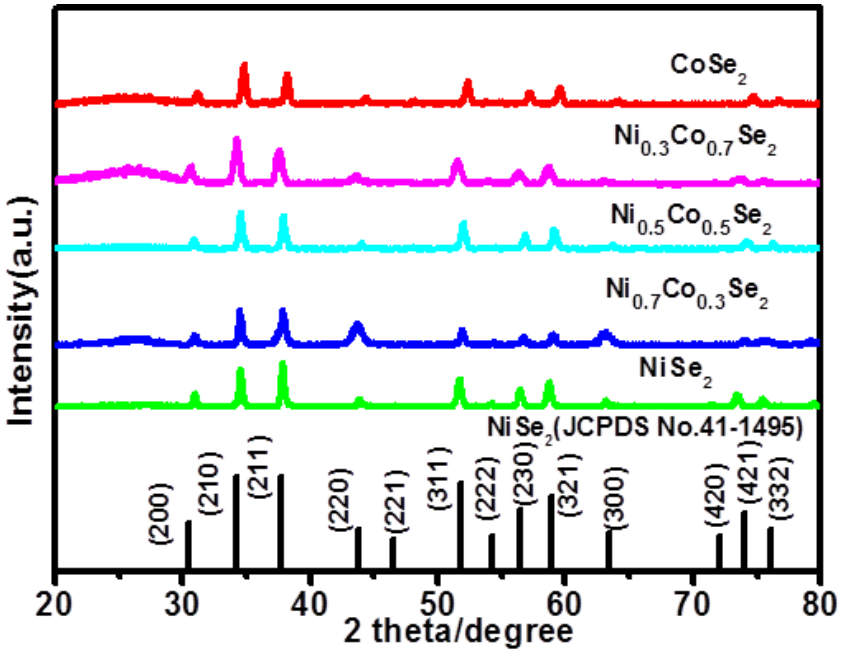

Figure S1. XRD patterns for $Ni_{0.5}Co_{0.5}Se_2$/CC, $Ni_{0.3}Co_{0.7}Se_2$/CC, $Ni_{0.7}Co_{0.3}Se_2$/CC, $CoSe_2$/CC and $NiSe_2$/CC

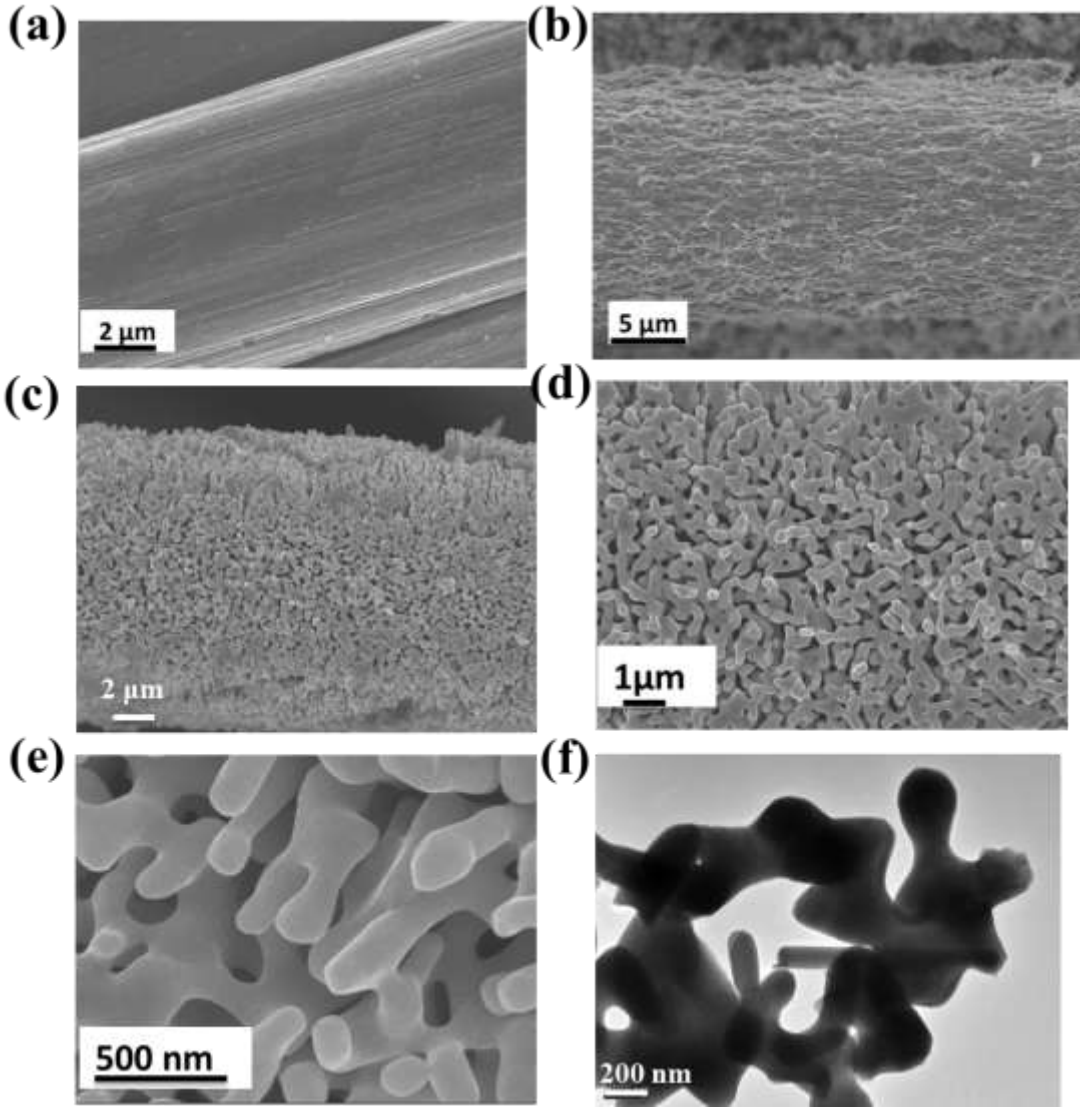

Figure S2. SEM images for the CC (a), $Ni_{0.5}Co_{0.5}(OH)_2$/CC (b-c) and its corresponding selenization $Ni_{0.5}Co_{0.5}Se_2$/CC (d-e); TEM image for $Ni_{0.5}Co_{0.5}Se_2$/CC (f).

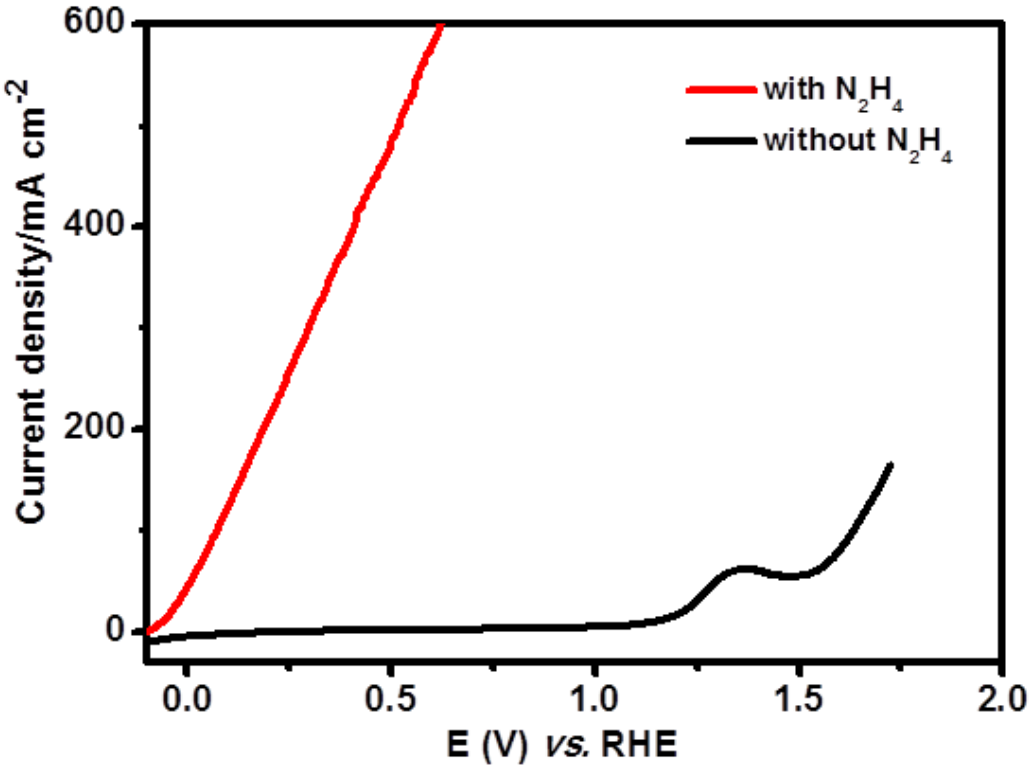

Figure S3. (a)Linear sweep voltammetry (LSV) curves of the representative $Ni_{0.5}Co_{0.5}Se_2$/CC for HzOR and OER in 1.0 M KOH

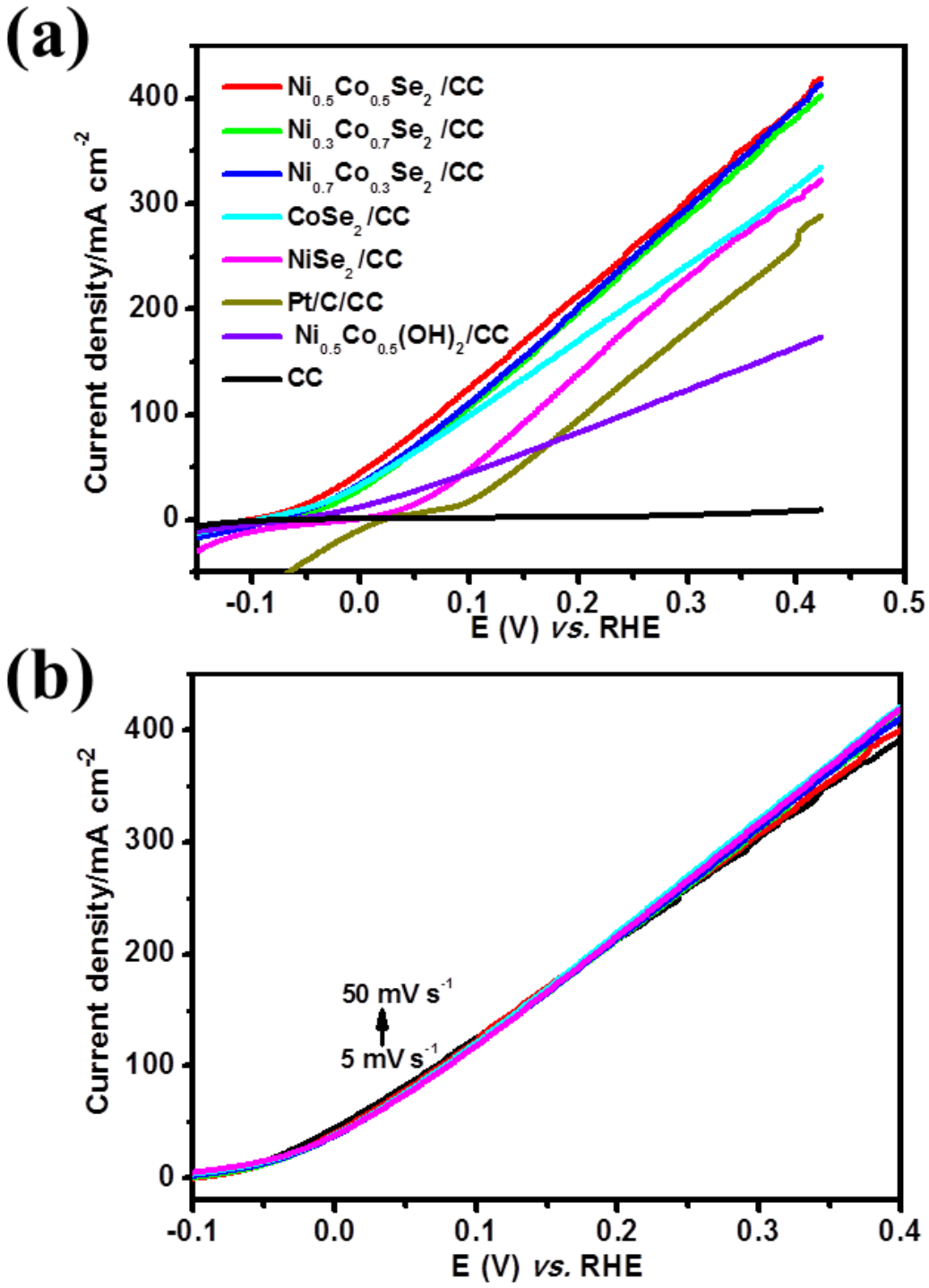

Figure S4. (a) LSV curves in 1 M KOH in presence of 0.5 M N_2H_4 at a scan rate of 5 mV s^{-1};(b) LSV curves of $Ni_{0.5}Co_{0.5}Se_2$/CC electrode in 1 M KOH with 0.5 M hydrazine at different scan

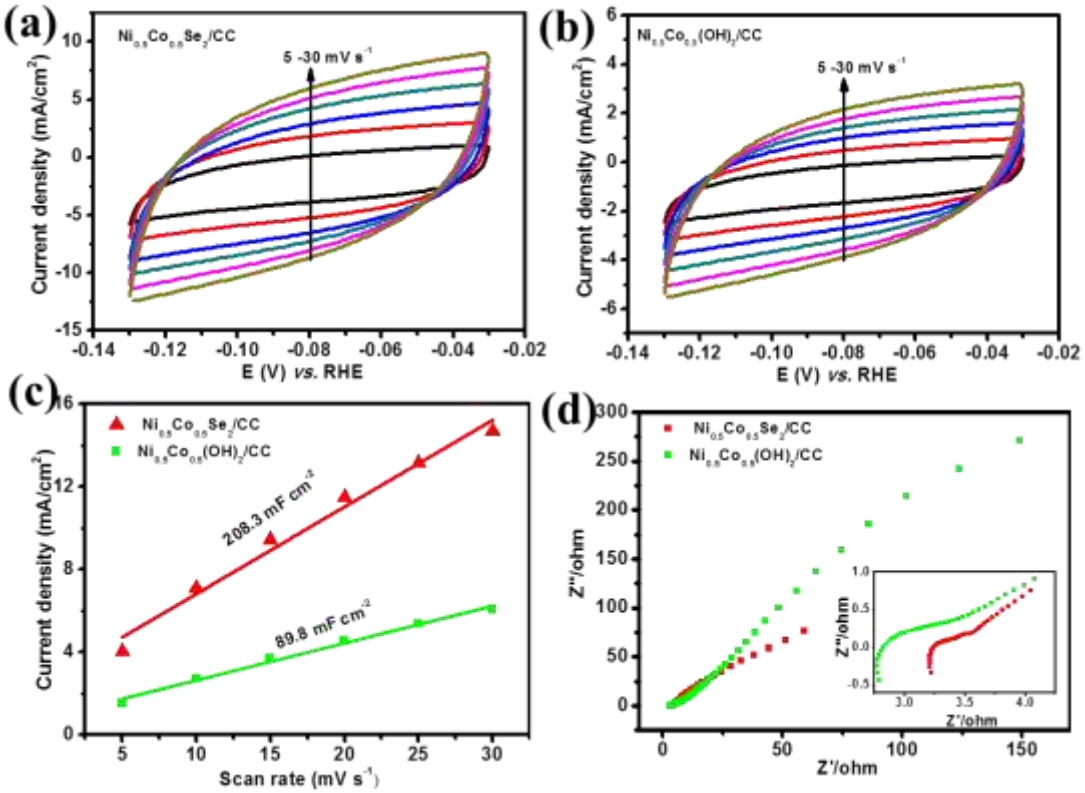

Figure S5. Electrochemical capacitance measurements for the estimation of the electrochemical active surface area of catalysts in 1.0 M KOH; Cyclic voltammograms of the $Ni_{0.5}Co_{0.5}Se_2$/CC (a) and $Ni_{0.5}Co_{0.5}(OH)_2$/CC (b) with scan rates ranging from 5 mV s^{-1} to 30 mV s^{-1} with an interval point of 5 mV s^{-1} , the scanning potential range is from -0.13 V to 0.03 V vs. RHE; the extraction of the double-layer capacitances of $Ni_{0.5}Co_{0.5}Se_2$/CC and $Ni_{0.5}Co_{0.5}(OH)_2$/CC, the C_{dl} was estimated by plotting j_a -j_c at -0.08 V (where j_c and j_a are the cathodic and anodic current densities, respectively) vs. RHE against the scan rate, where the slope was twice that of C_{dl}. (c); Nyquist plots for $Ni_{0.5}Co_{0.5}Se_2$/CC and $Ni_{0.5}Co_{0.5}(OH)_2$/CC in frequency range of 0.01- 10^5Hz (d)

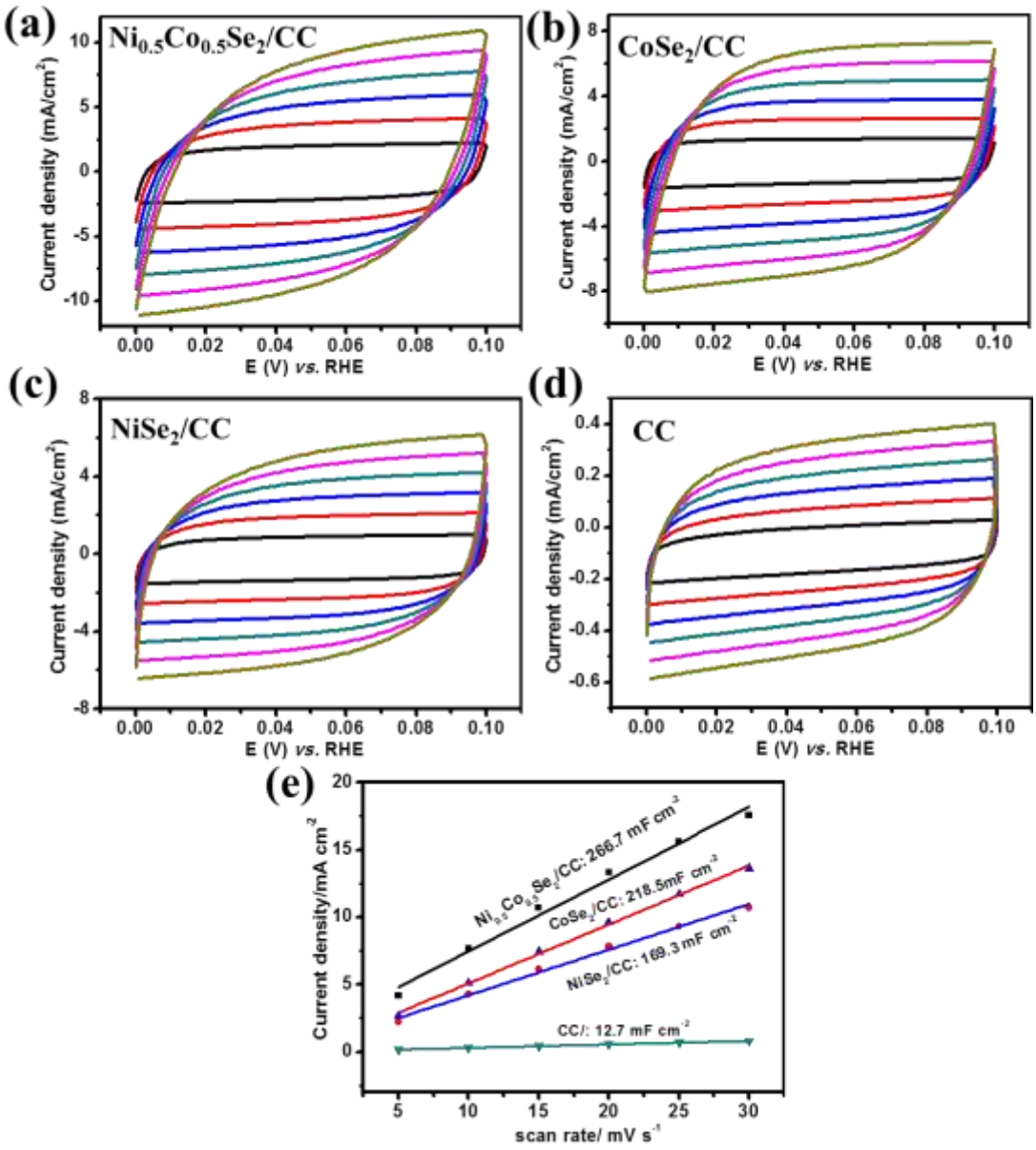

Figure S6. Electrochemical capacitance measurements for the estimation of the electrochemical active surface area of catalysts in 0.5 M H_2SO_4; Cyclic voltammograms of the $Ni_{0.5}Co_{0.5}Se_2$/CC (a), $CoSe_2$ (b), $NiSe_2$ (c) and CC (d) with scan rates ranging from 5 mV s^{-1} to 30 mV s^{-1} with an interval point of 5 mV s^{-1}, the scanning potential range is from 0 V to 0.1 V vs. RHE; the extraction of the double-layer capacitances of $Ni_{0.5}Co_{0.5}Se_2$/CC, $CoSe_2$, $NiSe_2$ and CC, the C_{dl} was estimated by plotting j_a -j_c at 0.05 V (where j_c and j_a are the cathodic and anodic current densities, respectively) vs. RHE against the scan rate, where the slope was twice that of C_{dl} (e)

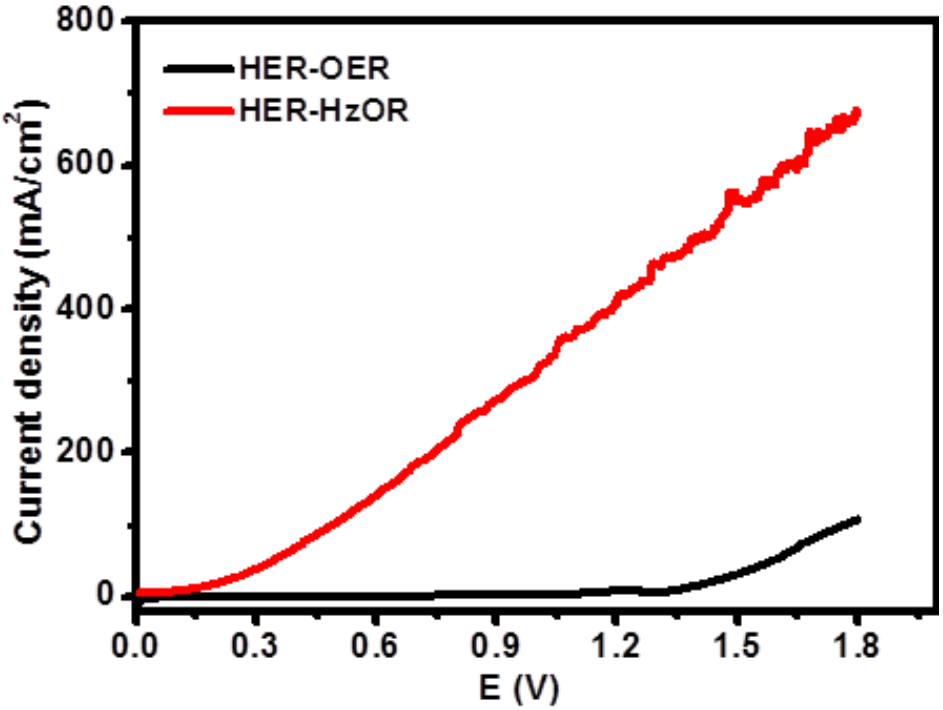

Figure S7. LSV curves of two-electrode system with $Ni_{0.5}Co_{0.5}Se_2$/CC as the bifunctional catalysts in 1.0 M KOH electrolyte

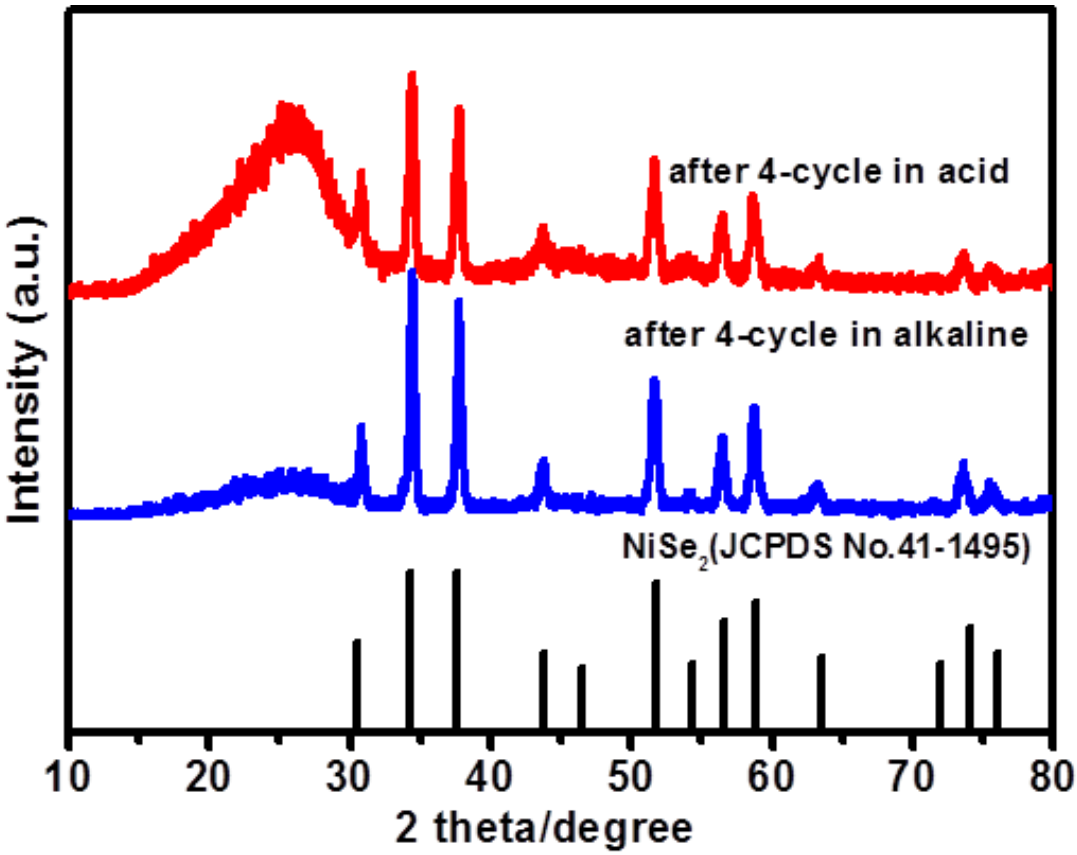

Figure S8. XRD of $Ni_{0.5}Co_{0.5}Se_2$/CC after 105 h in acid and in alkaline, respectively

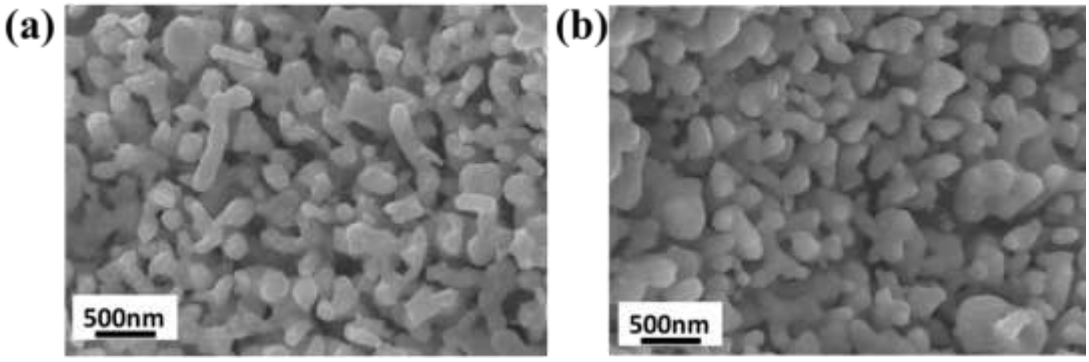

Figure S9. SEM images of $Ni_{0.5}Co_{0.5}Se_2$/CC after HER in acid (a) and HzOR (b) in alkaline, respectively

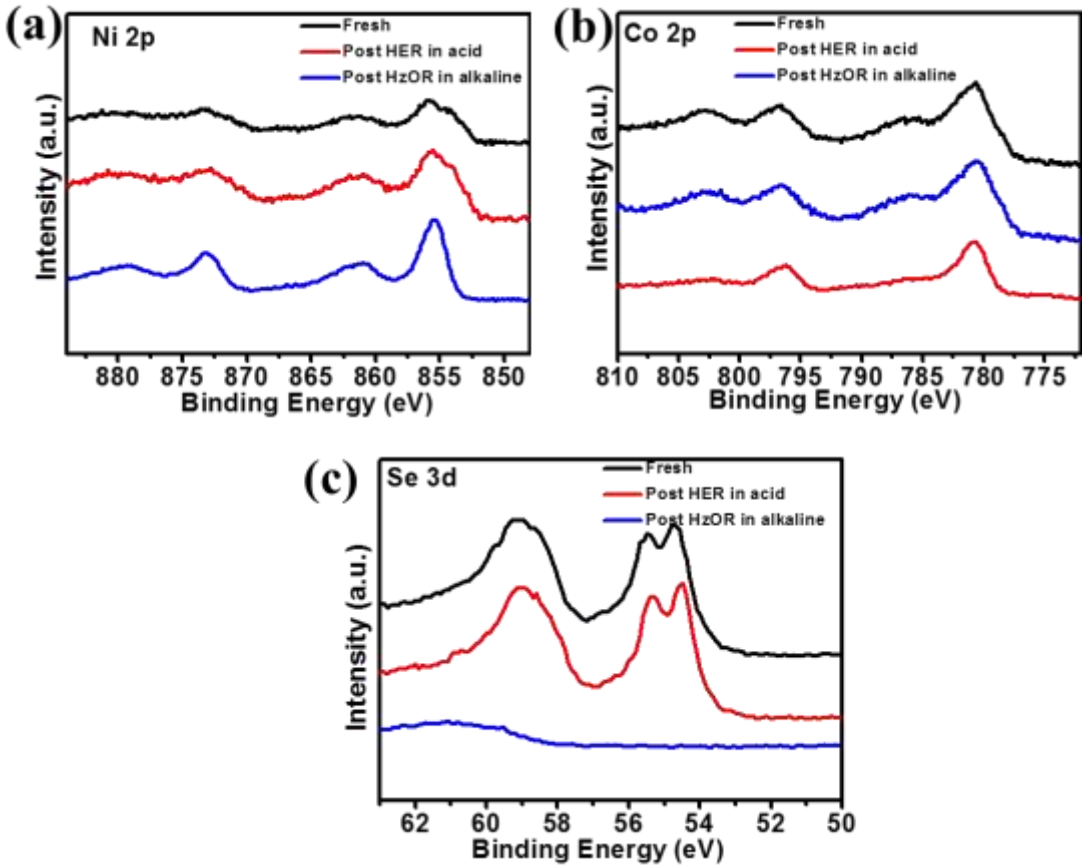

Figure S10. Comparison of high-resolution XPS spectra of (a) Ni 2p, (b) Co 2p, (c) Se 3d for the fresh, post-HER and post-HzOR $Ni_{0.5}Co_{0.5}Se_2$/CC samples.

Figure S11. Photograph of a red LED (about 1.8-2.2 V) powered by three HzOR-HER asymetric-electrolyte cell with $Ni_{0.5}Co_{0.5}Se_2$ as the electrodes

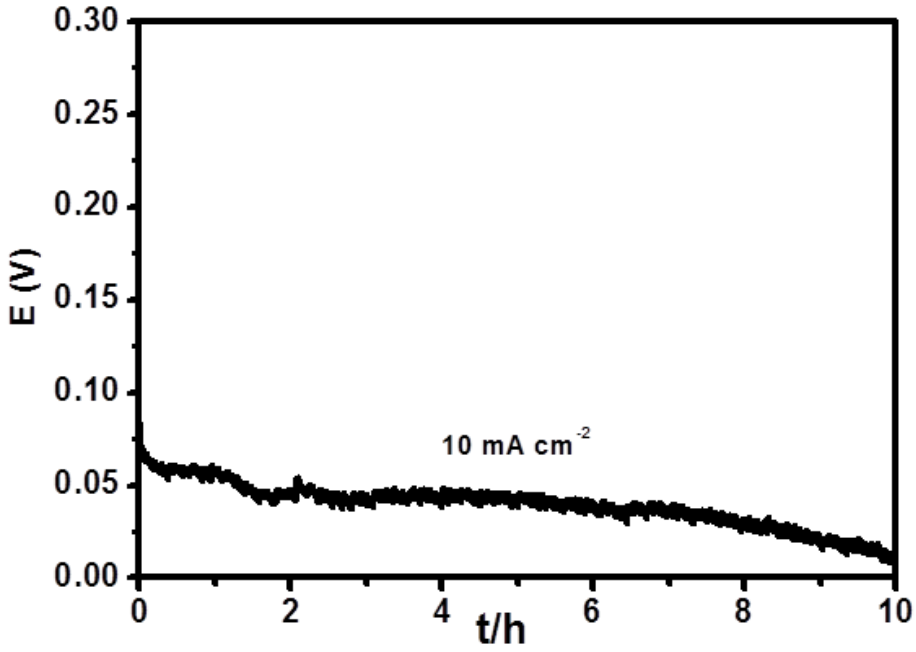

Figure S12. The asymetric-electrolyte hydrazine fuel cell discharging at constant-current of 10 mA cm^{-2}

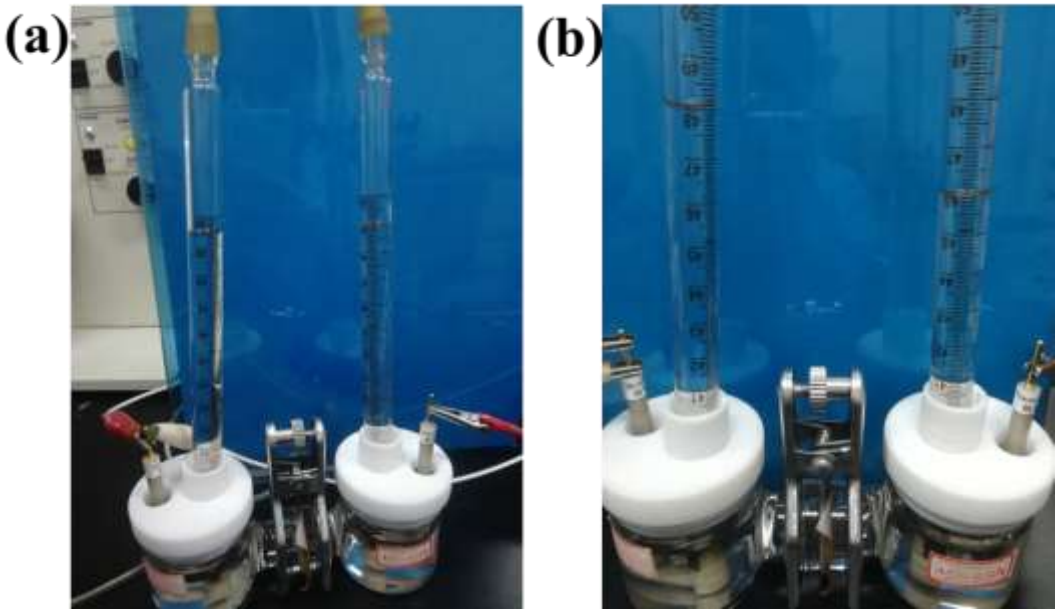

Figure S13. The device for measuring H_2 Faradaic Efficiency

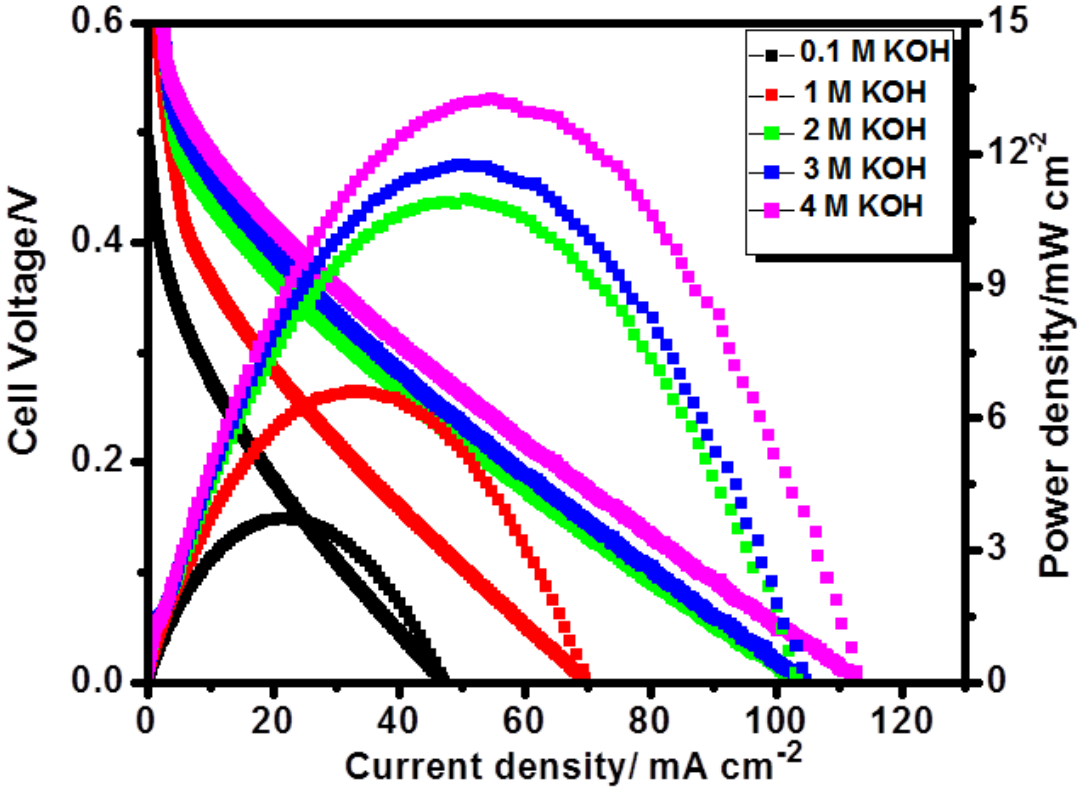

Figure S14. Cell performance polts with different KOH concentration in anode and 0.5 M H_2SO_4 in cathode with $Ni_{0.5}Co_{0.5}Se_2$/CC as both the anode and cathode at room temperature;

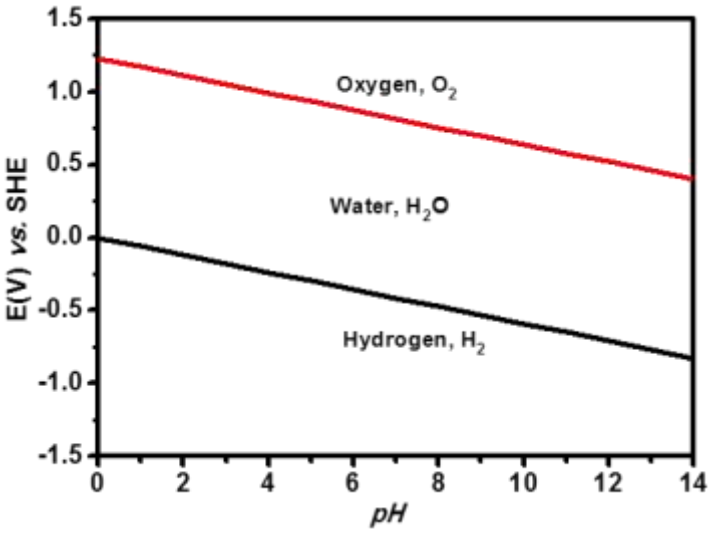

Figure S15. A pourbaix daigram of water with curves obtained by the Nernst equation (Equations 1 and 2)

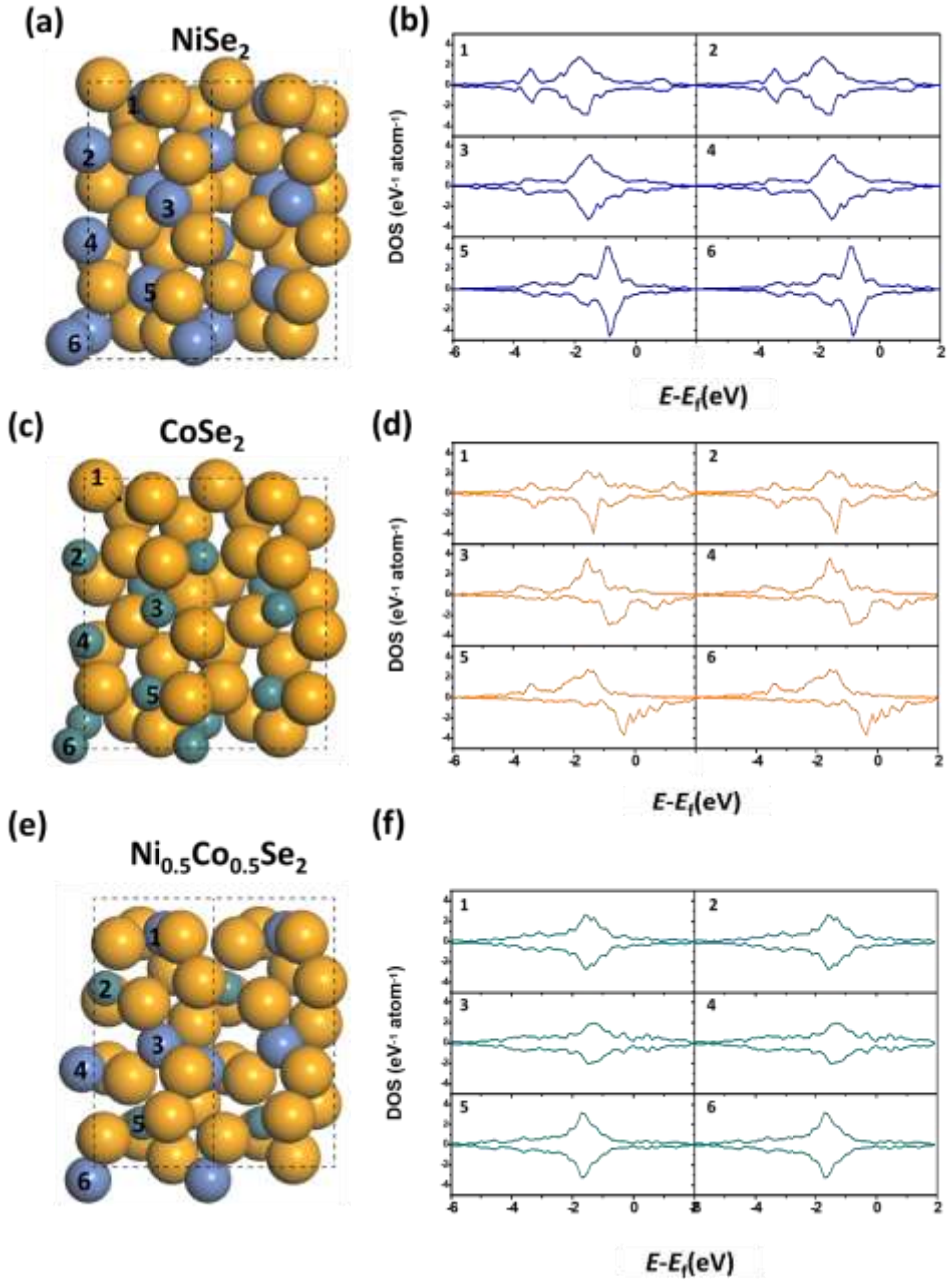

Figure S16. (a, c, d) the top views of the DFT optimized surfaces, where the associated numbers are the possible active sites. (b, d, f) The associated PDOS of these sites. The numbers give the site numbers.

5. Tables

Table S1. Comparison of electrochemical parameters for tranditional hydrazine fuel cell, water electrolysis, hydrazine oxidation assisted water electrolysis, and the hydrogen production hydrazine fuel cell

Reactions	**Input or output voltage (V)**	**Gibbs Free Energy (KJ mol^{-1})**	**H_2 production (mol)**	**References**
$N_2H_4 + O_2 \rightarrow N_2 + 2H_2O$	1.56 (output)	-602.07	0	3
$H_2O \rightarrow O_2 + 2H_2$	1.23 (input)	474.70	2	4
$N_2H_4 \rightarrow N_2 + 2H_2$	0.33(output)	-127.36	2	5
$N_2H_4 + H^+ + OH^- \rightarrow N_2 + 2H_2$	1.16 (output)	-447.69	2	This work

Table S2. Elemental compositions of the products obtained by ICP[a]

Ni/Co feed ratio	Ni/Co ratio in $Ni_{1-x}Co_x(OH)_2$	Ni/Co ratio in $Ni_{1-x}Co_xSe_2$
1/1	$Ni_{0.47}Co_{0.53}(OH)_2$ **Or $Ni_{0.5}Co_{0.5}(OH)_2$**	$Ni_{0.55}Co_{0.45}Se_2$ **Or $Ni_{0.5}Co_{0.5}Se_2$**
1/2	$Ni_{0.26}Co_{0.74}(OH)_2$ **Or $Ni_{0.3}Co_{0.7}(OH)_2$**	$Ni_{0.31}Co_{0.69}Se_2$ **Or $Ni_{0.3}Co_{0.7}Se_2$**
2/1	$Ni_{0.67}Co_{0.33}(OH)_2$ **Or $Ni_{0.7}Co_{0.3}(OH)_2$**	$Ni_{0.68}Co_{0.32}Se_2$ **Or $Ni_{0.7}Co_{0.3}Se_2$**

[a] The error in the ICP measurement was 5%

Table S3. Comparison of HzOR performance for these selenides in this work with other catalysts under alkaline conditions

Catalysts	Electrolytes	E (50 mA cm^{-2})/mV *vs.* RHE	References
Ni_2P/NF	1.0 M KOH + 0.5 M N_2H_4	-25	[5]
Cu film/CF	3.0 M NaOH + 1.0 M N_2H_4	358 [m]	[6]
Ni nano arrays	3.0 M KOH + 1.0 M N_2H_4	15 [m]	[7]
Ni nanoflowers	3.0 M KOH + 0.5 M N_2H_4	60 [m]	[8]
Cu nanowire arrays	3.0 M NaOH + 1.0M N_2H_4	310 [m]	[9]
Ni-Zn/NF	1.0 M NaOH + 0.1 M N_2H_4	20[m]	[10]
porous Ni-Cu alloy	3.0 M NaOH + 0.1M N_2H_4	130 [m]	[11]
FeP NA/NF	1.0 M KOH + 0.5 M N_2H_4	87	[12]
Cu_3P/CF	1.0 M KOH + 0.5 M N_2H_4	98	[13]
CoS_2/Ti mesh	1.0 M KOH + 0.1 M N_2H_4	65 [m]	[14]
Nanoporous Cu film/Cu plate	3.0 M NaOH + 0.1 M N_2H_4	311 [m]	[15]
Flower-like Co nano-particles/NF	1.0 M NaOH + 0.03 M N_2H_4	114 [m]	[16]
$CoSe_2$/NF	1.0 M KOH + 0.5 M N_2H_4	70 [m]	[17]
CoP/TiM	1.0 M KOH + 0.1 M N_2H_4	-30 [m]	[18]
$Ni_{0.5}Co_{0.5}Se_2$/CC	1.0 M KOH + 0.5 M N_2H_4	8	This work
$Ni_{0.3}Co_{0.7}Se_2$/CC		30	
$Ni_{0.7}Co_{0.3}Se_2$/CC		24	
$NiSe_2$/CC		28	
$CoSe_2$/CC		114	

CF: Cu foam

NF: Ni foam

CC: Carbon cloth

m: evaluated in its figures

Table S4. Lists of applied voltage for H_2 production from water electrolysis assisted by small molecules or biomass oxidation in recent reports

Catalysts	Anodic oxidation	Electrolytes	Applied voltage at 10 mA cm-2/(V)	Refs
Ni_3S_2/NF[d]	10 mM HMF	1.0 M KOH	1.46	[19]
Ni_2P NPA/NF[d]	10 mM HMF	1.0 M KOH	1.44	[20]
Co-P/CF[d]	10 mM HMF	1.0 M KOH	1.39[m]	[21]
hp-Ni[d]	Benzyl alcohol	1.0 M KOH	1.50	[22]
Ni_2P/Ni/NF[d]	30 mM furfural	1.0 M KOH	1.48	[23]
3D PdCu alloy NSs[d]	1.0 M Ethanol	1.0 M KOH	NG	[24]
Ultrathin Co_3O_4 NSs[d]	1.0 M Ethanol	1.0 M KOH	NG	[25]
$Zn_{0.08}Co_{0.92}P$[s]	0.5 M urea	1.0 M KOH	1.38	[26]
Ni_2P NF/CC[s]	0.5 M urea	1.0 M KOH	1.15 [m]	[27]
$MnO_2/MnCo_2O_4$/Ni[s]	0.5 M urea	1.0 M KOH	1.58	[28]
Small-sized MnO_2[s]	0.5 M urea	1.0 M KOH	1.41	[29]
CoS_2 NA/Ti [s]	0.3 M urea	1.0 M KOH	1.59	[30]
Ni_3N nanosheet/CC	0.33 M urea	1.0 M KOH	1.44	[31]
CuCl/rGO[d]	0.5 M urea	2.0 M KOH in anode and 0.5 M H_2SO_4 in cathode	0.83	[32]
$NiMoO_4$/NF	0.5 M urea	1.0 M KOH	1.38	[33]
$CoSe_2$/NF	0.5 M N_2H_4	1.0 M KOH	0.164	[17]
NiS_2/TiM	0.5 M N_2H_4	1.0 M KOH	0.3[m]	[34]
$Ni_{0.5}Co_{0.5}Se_2$	0.5 M N_2H_4	1.0 M KOH	0.14	This work
	0.5 M N_2H_4	1.0 M KOH in anode and 0.5 M H_2SO_4 in cathode	0	This work

CF: Cu foam
NF: Ni foam
CC: Carbon cloth
TiM: Ti mesh
m: evaluated in its figures

Table S5. The recorded data for Faradaic Efficiency of H_2 and its evolution rate at a current density of 10 mA cm^{-2}

t/s	V/mL	n/mol	EF	H_2 Evolution rate/μmol h^{-1}
424	0.5	2.04082E-05	0.928812091	173.2772
824	1	4.08163E-05	0.95586487	178.3236
1219	1.5	6.12245E-05	0.969195225	180.8107
1613	2	8.16327E-05	0.976605893	182.1933
2006	2.5	0.000102041	0.981596028	183.1244
2416	3	0.000122449	0.978020678	182.4571
2811	3.5	0.000142857	0.980688113	182.9545
3224	4	0.000163265	0.977211728	182.3058
3629	4.5	0.000183673	0.976673171	182.2052
4062	5	0.000204082	0.969513359	180.8703
4503	5.5	0.00022449	0.962020784	179.4724
4908	6	0.000244898	0.962876104	179.6318
5336	6.5	0.000265306	0.959447572	178.9921
5760	7	0.000285714	0.95719246	178.5713
6168	7.5	0.000306122	0.95772453	178.6704
6564	8	0.000326531	0.959942295	179.0846
6968	8.5	0.000346939	0.960803322	179.2452
7376	9	0.000367347	0.961048519	179.2908

Table S6. The zero-point energy (ZPE) values are calculated with the Phonon-5.0.2 module in espresso-5.0,[2] and the molecular entropy values are from Ref. 35. A pressure of 0.035 Bar is included in the entropy of gas-phased H_2O, for at 300 K, gas-phased H_2O and the liquid water reach equilibrium under this pressure.

Species	TS (eV)	ZPE (eV)
H_2(g)	0.41	0.27
N_2(g)	0.61	0.17
N_2H_4*	0	0.20
N_2H_3*	0	0.18
N_2H_2*	0	0.16
N_2H*	0	0.23
N_2*	0	0.22

6. References:

1. P. Giannozzi, S. B. N. Bonini, M. Calandra, R. Car, C. Cavazzoni, D. Ceresoli, G. L. Chiarotti, M. Cococcioni, I. Dabo, A. Dal Corso, S. Fabris, G. Fratesi, S. de Gironcoli, R. Gebauer, U. Gerstmann, C. Gougoussis, A. Kokalj, M. Lazzeri, L. MartinSamos, N. Marzari, F. Mauri, R. Mazzarello, S. Paolini, A. Pasquarello, L. Paulatto, C. Sbraccia, S. Scandolo, G. Sclauzero, A. P. Seitsonen, A. Smogunov, P. Umari, R. M. Wentzcovitch, *J. Phys.: Condens. Matter.*, 2009, **21**, 395502
2. L. Zhou,, M. Shao, C. Zhang, J. Zhao, S. He, D Rao, X. Duan, *Adv. Mater.*, 2017, **29,** 164080
3 A. Serov, C. Kwak, *Appl. Catal. B Environ.* 2010, **98**, 1-9.
4 M. Fang, G. F. Dong, R. J. Wei, J. C. Ho, Adv. Energy Mater., 2017, 7, 1700559.
5. C. Tang, R. Zhang, W. Lu, Z. Wang, D. Liu, S. Hao, G. Du, A. M. Asiri and X. Sun, *Angew. Chem. Ger. Edit.*, 2017, **129**, 860-864.
6. Z. Lu, M. Sun, T. Xu, Y. Li, W. Xu, Z. Chang, Y. Ding, X. Sun and L. Jiang, *Adv. Mater.*, 2015, **27**, 2361-2366.
7. Y. Kuang, G. Feng, P. Li, Y. Bi, Y. Li and X. Sun, *Angew. Chem. Ger. Edit.*, 2016, **128**, 703-707.
8. G. Feng, Y. Kuang, Y. Li and X. Sun, *Nano Research*, 2015, **8**, 3365-3371.
9. J. Huang, S. Zhao, W. Chen, Y. Zhou, X. Yang, Y. Zhu and C. Li, *Nanoscale*, 2016, **8**, 5810-5814.
10. L.-S. Wu, H.-B. Dai, X.-P. Wen and P. Wang, *ChemElectroChem*, 2017, **4**, 1944-1949.
11. M. Sun, Z. Lu, L. Luo, Z. Chang and X. Sun, *Nanoscale*, 2016, **8**, 1479-1484.
12. L. Zhang, D. Liu, S. Hao, L. Xie, F. Qu, G. Du, A. M. Asiri and X. Sun, *ChemistrySelect*, 2017, **2**, 3401-3407.
13. M. Liu, R. Zhang, L. Zhang, D. Liu, S. Hao, G. Du, A. M. Asiri, R. Kong and X. Sun, *Inorg. Chem. Front.*, 2017, **4**, 420-423.
14. X. Ma, J. Wang, D. Liu, R. Kong, S. Hao, G. Du, A. M. Asiri and X. Sun, *New J. Chem.*, 2017, **41**, 4754-4757.
15. F. Jia, J. Zhao and X. Yu, *J. Power Sources*, 2013, **222**, 135-139.
16. F. Yang, K. Cheng, G. Wang and D. Cao, *J. Electroanal. Chem.*, 2015, **756**, 186-192.
17. J. Y. Zhang, H. Wang, Y. Tian, Y. Yan, Q. Xue, T. He, H. Liu, C. Wang, Y. Chen and B. Y. Xia, *Angew. Chem. Int. Ed.*, 2018, **57**, 7649-7653.
18. J. Wang, R. Kong, A. M. Asiri and X. Sun, *ChemElectroChem*, 2017, **4**, 481-484.
19. B. You, X. Liu, N. Jiang and Y. Sun, *J. Am. Chem. Soc.*, 2016, **138**, 13639-13646.
20. B. You, N. Jiang, X. Liu and Y. Sun, *Angew. Chem. Ger. Edit.*, 2016, **128**, 10067-10071.
21. N. Jiang, B. You, R. Boonstra, I. M. Terrero Rodriguez and Y. Sun, *ACS Energy Lett.*, 2016, **1**, 386-390.
22. B. You, X. Liu, X. Liu and Y. Sun, *ACS Catal.*, 2017, **7**, 4564-4570.
23. N. Jiang, X. Liu, J. Dong, B. You, X. Liu and Y. Sun, *ChemNanoMat*, 2017, **3**, 491-495.
24. X. Zhao, L. Dai, Q. Qin, F. Pei, C. Hu and N. Zheng, *Small*, 2017, **13**, 1602970.
25. L. Dai, Q. Qin, X. Zhao, C. Xu, C. Hu, S. Mo, Y. O. Wang, S. Lin, Z. Tang and N. Zheng, *ACS Cent. Sci.*, 2016, **2**, 538-544.
26. T. T. Liu, D. N. Liu, F. L. Qu, D. X. Wang, L. Zhang, R. X. Ge, S. Hao, Y. J. Ma, G. Du,

A. M. Asiri, L. Chen and X. P. Sun, *Adv. Energy Mater.*, 2017, **7**, 1700020.
27. D. Liu, T. Liu, L. Zhang, F. Qu, G. Du, A. M. Asiri and X. Sun, *J. Mater. Chem. A*, 2017, **5**, 3208-3213.
28. C. Xiao, S. Li, X. Zhang and D. R. MacFarlane, *J. Mater. Chem. A*, 2017, **5**, 7825-7832.
29. S. Chen, J. Duan, A. Vasileff and S. Z. Qiao, *Angew. Chem. Ger. Edit.*, 2016, **128**, 3868-3872.
30. S. Wei, X. Wang, J. Wang, X. Sun, L. Cui, W. Yang, Y. Zheng and J. Liu, *Electrochim Acta*, 2017, **246**, 776-782.
31. Q. Liu, L. Xie, F. Qu, Z. Liu, G. Du, A. M. Asiri and X. Sun, *Inorg. Chem. Front.*, 2017, **4**, 1120-1124.
32. G. Wang, J. Chen, Y. Li, J. Jia, P. Cai and Z. Wen, *Chem. Commun.*, 2018, **54**, 2603-2606.
33. Z.-Y. Yu, C.-C. Lang, M.-R. Gao, Y. Chen, Q.-Q. Fu, Y. Duan and S.-H. Yu, *Energ. Environ. Sci.*, 2018, **11**, 1890-1897.
34. J. Wang, X. Ma, T. Liu, D. Liu, S. Hao, G. Du, R. Kong, A. M. Asiri and X. Sun, *Mater. Today Energy*, 2017, **3**, 9-14.
35. Weast, R. C., Ed. CRC Handbook of Chemistry and Physics, 49th ed.; The Chemical Rubber Company: Cleveland, OH, 1968-1969; p D109.